投稿論文(英文)
PAPERS

Structural Eng./Earthquake Eng. Vol. 10, No. 1, 1s—12s, April 1993
Japan Society of Civil Engineers (Proc. of JSCE No. 465/ I—23)

ACTIVE OPTIMAL CONTROL OF ABRIDGE TOWER AGAINST GALLOPING USING AN OPTIMAL OBSERVER

S.M. Shahid ALAM*, Shunsuke BABA**
and Masaru MATSUMOTO***

An active optimal control algorithm is presented for the suppression of self-excited vibration such as galloping in towers of long span bridges. Quasi-steady theory is applied to model the aerodynamic forces and multimode response is considered to observe the intermode interaction. Gust load is considered as a random phenomenon and modeled by the power spectra of the along and across wind fluctuating velocities. The possible error in the response prediction, due to uncertainty in the quasi-steady theory and the random gust phenomenon, is rectified by the introduction of an observer. An optimal observer is used to minimize its effect on the increment of the objective function. The effect of the observer on the change in system parameter and gust intensity is examined, also the time delay effect on the performance of the controller is investigated.

Key Words : *galloping, multimodal interaction, active control, optimal observer*

1. INTRODUCTION

With the increasing need of longer span, the suspension and cable stayed bridges are becoming more and more flexible and consequently more susceptible to aerodynamic forces. The towers of such structures, which are usually aerodynamically bluff, show instability above certain wind velocities. These instabilities result in vortex induced motion and galloping along with buffeting due to turbulence in the wind. As the vortex induced motion is small as compared to the galloping, in this study, we have restricted our discussion only to galloping and buffeting related vibrations.

In the past, various passive means have been employed to control these undesirable vibrations. The most effective of them is to artificially increase the damping of the structure. Fujino et al.[1] applied Tuned Mass Damper (TMD) for this problem and increased the damping of the fundamental mode of the structure by tuning it with the damper. However, their results showed that TMD is not so effective at high wind velocities, where higher modes are excited. Furthermore, their work did not include the multimode galloping[2)-4)] suppression problem. The limitation of passive control provides sufficient reason to think of a suitable active vibration control scheme. To the best of authors knowledge, the active control of galloping related vibration has not been studied yet. It is the purpose of this study to present a suitable active control algorithm for a structure galloping in a gusty wind. Contrary to direct velocity feed back (DVFB) control, which is simpler than other approaches[5], the proposed scheme suggests an optimal regulator control with an observer. The reason is that DVFB, although simple in application, is believed to be a low authority control[6]. On the other hand a controller with an observer results in a qualitative control, which in authors opinion is one of the prerequisites of an active control of such important structures like long span bridges. The use of an observer increases the robustness against uncertainties like aerodynamic load prediction, gust load, the spontaneous changes in system parameters such as change in mass and stiffness matrices, which are due to the aging of the structure or the effect of occasional unsymmetric mass distribution etc[3]. Although, the scheme is applicable to either a single or multimode galloping control, the emphasis is put on a multimode galloping problem. A particular structure is selected as the illustrative example to observe the multimode galloping behavior under smooth flow and also to see its response under the action of a control force in a gusty wind.

This paper is structured as follows. In Section 2.1, the equation of motion of a continuous structure subjected to galloping in a gusty wind and under the action of control forces is formulated. The self exciting force is modeled by the quasi-steady theory with a seventh order polynomial showing the intermode interaction. The gust load is considered as a random phenomenon and modeled by the along and across wind fluctuating velocity power spectra[7),8)] as discussed in Section 2.2. In Section 2.3, the second order differential equation

* Graduate Student, Dept. of Civil Engineering, Nagoya University, Furo-cho, Chikusa-ku, Nagoya 464-01
** Associate Professor, Dept. of Civil Engineering, Nagoya University
*** Associate Professor, Dept. of Civil Engineering, Kyoto University

of motion is modified to a finite difference equation suitable for digital control. An expression for the optimal control force using an optimal regulator scheme is derived in Section 3. The introduction of the observer is described in Section 4. The increase in the objective function due to the introduction of the observer is minimized by using an optimal observer as discussed in Section 5. Section 6 gives a layout plan for the control system with the observer. In Section 7, an illustrative example is solved to observe the galloping phenomenon and its control. Finally, Section 8 contains the conclusions drawn from this study.

2. BASIC ANALYSIS

(1) Equation of Motion

Consider a bluff continuous body like a bridge tower, under the action of a strong wind and control forces. The equation of motion perpendicular to the direction of the wind has been formulated as

$$m(z)\frac{\partial^2 y(z,t)}{\partial t^2}+c(z)\frac{\partial y(z,t)}{\partial t}+\frac{\partial^2}{\partial z^2}\left[EI(z)\frac{\partial^2 y(z,t)}{\partial z^2}\right]=\sum_{j=1}^{r}u_j(t)\delta(z-a_j)+F_{se}(z,t)+F_b(z,t) \quad \cdots\cdots(1)$$

where z is the height from the ground and t is the time. $m(z)$, $c(z)$ and $I(z)$ are the mass, damping and the moment of inertia of the structure per unit length respectively. E is the modulus of elasticity of the structural material and $y(z,t)$ is the displacement function. Here r is the number of actuators and $\delta(z-a_j)$ is the Dirac delta function, which gives the location of the j-th actuator $u_j(t)$, placed at height a_j. $F_{se}(z,t)$ and $F_b(z,t)$ are the self-exciting and the buffeting forces per unit length respectively.

The self-exciting force appearing in Eq. (1) can be modeled by the quasi-steady theory[9] which has been verified[10] at velocities considerably higher than the vortex shedding velocities. Hence according to quasi-steady theory

$$F_{se}(z,t)=\frac{1}{2}\rho hV^2(z)\sum_i A_i\left(\frac{\partial y(z,t)}{\partial t}/V(z)\right)^i \quad i=1,3,5,7 \quad \cdots\cdots(2)$$

Here ρ is the air density and h is a characteristic dimension, which is taken as the dimension of one of the legs of the tower perpendicular to the wind direction. $V(z)$ is the mean velocity of air and A_i is the aerodynamic coefficient.

The buffeting force appearing in Eq. (1) can be modeled as[11]

$$F_b(z,t)=\frac{1}{2}\rho hV^2(z)\left[C_L\left(2\frac{v_b(z,t)}{V(z)}\right)+C_L'\left(\frac{w_b(z,t)}{V(z)}\right)\right] \quad \cdots\cdots(3)$$

where $v_b(z,t)$ and $w_b(z,t)$ are along and across wind fluctuating velocities. C_L is the lift coefficient and $C_L'=dC_L/d\alpha$. where α is the static angle of attack. The drag term of Eq. (3) in reference[11] is neglected, as it is very small as compared to C_L'. The quantities C_L and C_L' etc. are determined experimentally for a particular cross section of the structure[12]. To be consistent with Eq. (2), we have again defined the characteristic dimension as h in Eq. (3).

Let the displacement function $y(z,t)$ and the mean velocity of air $V(z)$ are expressed as

$$y(z,t)=\sum_{s=1}^{\infty}\Psi_s(z)q_s(t) \quad \cdots\cdots(4a)$$

$$V(z)=V_0v(z)=V_0\left(\frac{z}{z_0}\right)^p \quad \cdots\cdots(4b)$$

Here $\Psi_s(z)$ and $q_s(t)$ are the mode shape and the generalized co-ordinate of the s-th mode respectively. $v(z)$ is the velocity distribution function and V_0 is the mean wind velocity at the reference height z_0 (usually 10 m). p is a constant depending on the topographic condition. Substituting Eqs. (2) and (4) in Eq. (1), multiplying the resulting equation by $\Psi_n(z)$ and integrating over the full height l of the structure, the equation of n-th mode is given by

$$\int_0^l m(z)\Psi_n^2(z)dz[\ddot{q}_n(t)+2\beta_n\omega_n\dot{q}_n(t)+\omega_n^2q_n(t)]=\int_0^l\Psi_n(z)\left[\sum_{j=1}^{r}u_j(t)\delta(z-a_j)\right]dz+\frac{1}{2}\rho h\left\{\sum_i A_iV_0^{2-i}\int_0^l v^{2-i}(z)\Psi_n(z)\left[\sum_{s=1}^{\infty}\Psi_s(z)\dot{q}_s(t)\right]^i dz\right\}+\int_0^l F_b(z,t)\Psi_n(z)dz \quad i=1,3,5,7 \quad \cdots\cdots(5)$$

Eq. (5) is a general equation and represent the coupling of the aeroelastic terms for infinite modes. Here ω_n and β_n are the circular frequency and the damping ratio of the n-th mode respectively. The intertial, mass and damping terms on the left hand side of Eq. (5) are linear and decoupled, also the buffeting force term on the right hand side of Eq. (5) is assumed to be uncoupled[13] whereas the aeroelastic force term which is nonlinear, is the only term which remains coupled. For the sake of simplicity, we have limited our study to only two modes, *i.e.* we have considered the intermode

interaction between only two modes. Let these modes are denoted as ζ and η ($\omega_\zeta \leq \omega_\eta$), Eq. (5) is then written as

$$\ddot{q}_n(t)+2\beta_n\omega_n\dot{q}_n(t)+\omega_n^2 q_n(t)=\sum_{j=1}^{r}\frac{C_{U,nj}}{m_n}u_j(t)+\frac{2\mu_n}{h}\{f_{en}(\dot{q})+f_{bn}(t)\} \quad \cdots\cdots(6)$$

where m_n and μ_n are the equivalent mass per unit length and the mass ratio for the n-th mode, and are given as

$$m_n=\frac{\int_0^l m(z)\Psi_n^2(z)dz}{D_n} \quad \cdots\cdots(7a)$$

$$\mu_n=\frac{\rho h^2}{4m_n} \quad \cdots\cdots(7b)$$

where

$$D_n=\int_0^l \Psi_n^2(z)dz \qquad n=\zeta,\eta$$

and $C_{U,nj}$ is the coefficient of j-th controller corresponding to n-th mode, and is given as

$$C_{U,nj}=\Psi_n(a_j)/D_n \quad \cdots\cdots(7c)$$

The aerodynamic force term $f_{en}(\dot{q})$ in Eq. (6) is given as

$$f_{en}(\dot{q})=A_1V_0C_{A,n1}\dot{q}_n(t)+A_3V_0^{-1}\sum_{k=2}^{5}\binom{3}{k-2}C_{A,nk}\dot{q}_\zeta^{5-k}(t)\dot{q}_\eta^{k-2}(t)+A_5V_0^{-3}\sum_{k=6}^{11}\binom{5}{k-6}C_{A,nk}\dot{q}_\zeta^{11-k}(t)\dot{q}_\eta^{k-6}(t)+A_7V_0^{-5}\sum_{k=12}^{19}\binom{7}{k-12}C_{A,nk}\dot{q}_\zeta^{19-k}(t)\dot{q}_\eta^{k-12}(t) \quad \cdots\cdots(7d)$$

where n and k describe the mode number and the coefficient number respectively, whereas the coefficients $C_{A,nk}$ are given as follows

$$C_{A,nk}=\int_0^l v(z)\Psi_n^2(z)dz/D_n, \qquad k=1$$

$$C_{A,nk}=\int_0^l v^{-1}(z)\Psi_\zeta^{7-\xi-k}(z)\Psi_\eta^{\xi+k-3}(z)dz/D_n, \qquad k=2,3,4,5$$

$$C_{A,nk}=\int_0^l v^{-3}(z)\Psi_\zeta^{13-\xi-k}(z)\Psi_\eta^{\xi+k-7}(z)dz/D_n, \qquad k=6,7,\cdots 11$$

$$C_{A,nk}=\int_0^l v^{-5}(z)\Psi_\zeta^{21-\xi-k}(z)\Psi_\eta^{\xi+k-13}(z)dz/D_n, \qquad k=12,13,\cdots 19$$

when $n=\zeta \Rightarrow \xi=1$ and when $n=\eta \Rightarrow \xi=2$.

The buffeting force term $f_{bn}(t)$ in Eq.(6) is given as[12)-15)]

$$f_{bn}(t)=(2V_0C_L)\left[\sqrt{2}\sum_{j=1}^{N}\left[S_{vv}(\omega_j)|\gamma_1(\omega_j)|^2\cdot|J_n(\omega_j)|^2\Delta\omega\right]^{\frac{1}{2}}\cos(\omega_j t+\phi_j)\right]+(V_0C_L')\left[\sqrt{2}\sum_{j=1}^{N}\left[S_{ww}(\omega_j)|\gamma_2(\omega_j)|^2\cdot|J_n(\omega_j)|^2\Delta\omega\right]^{\frac{1}{2}}\cos(\omega_j t+\phi_j)\right] \quad \cdots(7e)$$

where $S_{vv}(\omega_j)$ and $S_{ww}(\omega_j)$ are the one sided spectra of the along and across wind fluctuating velocity components. Also $\omega_j=(j-0.5)\Delta\omega$ and $\Delta\omega=\omega_u/N$, where ω_u is the upper cutoff frequency, N is the number of sampling. ϕ_j and ϕ_j are the random phase angles uniformly distributed between 0 and 2π. The joint acceptance function $|J_n(\omega_j)|^2$ and the aerodynamic admittances $|\gamma_1(\omega_j)|^2$ and $|\gamma_2(\omega_j)|^2$ in Eq.(7e) are defined in Appendix 1.

(2) Power Spectra

The power spectral density for the along wind velocity fluctuation $S_{vv}(\omega_j,z)$ is given as[7),12)]

$$S_{vv}(\omega_j,z)\frac{6K_1KV_0^2}{2\pi b_1[1+(\omega_j/2\pi b_1)^2]^{\frac{5}{6}}} \quad \cdots\cdots(8a)$$

in which

$$K_1=0.4751,\ b_1=K_2(KV_0^2)^{-\frac{3}{2}}V_0^4\left(\frac{pK}{z_0}\right)\left(\frac{z}{z_0}\right)^{4p-1},$$

$$K_2=1.169\times10^{-2}$$

where K is the surface drag coefficient.

The power spectral density for the across wind velocity fluctuation is given as[8)]

$$S_{ww}(\omega_j,z)=\frac{17KV_0^2z}{2\pi V(z)[1+\{9.5\omega_j z/2\pi V(z)\}]^{\frac{5}{3}}} \quad \cdots\cdots(8b)$$

(3) State Equation

From Eq. (6), the equation of motion for the two selected modes ζ and η is given as

$$\ddot{\boldsymbol{Q}}+\boldsymbol{C}\dot{\boldsymbol{Q}}+\boldsymbol{K}\boldsymbol{Q}=\boldsymbol{H}\boldsymbol{U}+\boldsymbol{S}\{\boldsymbol{F}_e(\dot{q})+\boldsymbol{F}_b(t)\} \quad \cdots\cdots(9)$$

where $\boldsymbol{Q}$ is the modal co-ordinate vector of size 2×1. $\boldsymbol{U}$ is the control force of size $r\times1$ and $\boldsymbol{F}_e(\dot{q})$ and $\boldsymbol{F}_b(t)$ are the modal force vectors of size 2×1. $\boldsymbol{C}$ and $\boldsymbol{K}$ are the damping and stiffness matrices of size 2×2. $\boldsymbol{H}$ and $\boldsymbol{S}$ are the coefficient matrices of size $2\times r$ and 2×2 respectively. These matrices are given as

$$\boldsymbol{Q}=\begin{Bmatrix}q_\zeta(t)\\q_\eta(t)\end{Bmatrix},\quad \boldsymbol{U}^T=\{u_1\cdots\cdots u_r\}^T,$$

$$\boldsymbol{F}_e(\dot{q})=\begin{Bmatrix}f_{e\zeta}(\dot{q})\\f_{e\eta}(\dot{q})\end{Bmatrix},\quad \boldsymbol{F}_b(t)=\begin{Bmatrix}f_{b\zeta}(t)\\f_{b\eta}(t)\end{Bmatrix},$$

$$K=\begin{bmatrix}\omega_\xi^2 & 0\\ 0 & \omega_\eta^2\end{bmatrix},\quad H=\begin{Bmatrix}C_{U,\zeta 1}/m_\zeta & \cdots & C_{U,\zeta r}/m_\zeta\\ C_{U,\eta 1}/m_\eta & \cdots & C_{U,\eta r}/m_\eta\end{Bmatrix},$$

$$C=\begin{bmatrix}2\beta_\zeta\omega_\zeta & 0\\ 0 & 2\beta_\eta\omega_\eta\end{bmatrix}\quad\text{and}\quad S=\begin{bmatrix}2\mu_\zeta/h & 0\\ 0 & 2\mu_\eta/h\end{bmatrix}$$

Eq. (9) is modified to a first order differential equation as follows,

$$\dot{\boldsymbol{Q}}^*=\boldsymbol{A}\boldsymbol{Q}^*+\boldsymbol{B}\boldsymbol{U}+\boldsymbol{D}\{\boldsymbol{F}_e(\dot{q})+\boldsymbol{F}_b(t)\}\quad\cdots\cdots(10)$$

where $\boldsymbol{Q}^*$ is a state vector of size 4×1. $\boldsymbol{A}$,$\boldsymbol{B}$ and $\boldsymbol{D}$ are the coefficient matrices of size 4×4, $4\times r$ and 4×2 respectively and are given as

$$\boldsymbol{Q}^*=\begin{Bmatrix}\dot{\boldsymbol{Q}}\\ \boldsymbol{Q}\end{Bmatrix},\quad \boldsymbol{A}=\begin{bmatrix}-\boldsymbol{C} & -\boldsymbol{K}\\ \boldsymbol{I} & 0\end{bmatrix},$$

$$\boldsymbol{B}=\begin{Bmatrix}\boldsymbol{H}\\ 0\end{Bmatrix}\quad\text{and}\quad \boldsymbol{D}=\begin{Bmatrix}\boldsymbol{S}\\ 0\end{Bmatrix}$$

It is noted that because of the velocity dependent self-exciting forces, Eq. (10) is nonlinear. The effect of nonlinearity is avoided by assuming $\boldsymbol{F}_e(\dot{q})\equiv\boldsymbol{F}_e^{old}$, where $\boldsymbol{F}_e^{old}$ is a known force which is equal to the aeroelastic force $\boldsymbol{F}_e(\dot{q})$ at time $t'=t-\Delta t$, where Δt is the sampling time used in the discretization of differential equation, which is discussed in the following paragraphs. This assumption is justified, provided that the sampling time is small and the velocity changes are gradual. With this consideration the state Eq. (10) is modified as follows

$$\dot{\boldsymbol{Q}}^*=\boldsymbol{A}\boldsymbol{Q}^*+\boldsymbol{B}\boldsymbol{U}+\boldsymbol{D}(\boldsymbol{F}_e^{old}+\boldsymbol{F}_b)\quad\cdots\cdots(11)$$

To check the validity of the above assumption a nonlinear step by step numerical integration procedure (Newmark-β method) is used. It is found that the responses calculated from Eq. (11) and Eq. (10) are almost identical, when the sampling time Δt is sufficiently small. Discretization of Eq. (11) results in the following state equation[16]

$$\boldsymbol{Q}_{i+1}^*=\boldsymbol{A}^*\boldsymbol{Q}_i^*+\boldsymbol{C}^*\boldsymbol{U}_i+\boldsymbol{D}^*\boldsymbol{F}_{e,i-1}+\boldsymbol{D}^*\boldsymbol{F}_{b,i}\quad\cdots\cdots(12)$$

where

$$\boldsymbol{A}^*=\exp(\boldsymbol{A}\Delta t),\quad \boldsymbol{C}^*=(\boldsymbol{A}^*-\boldsymbol{I})\boldsymbol{A}^{-1}\boldsymbol{B}\ \text{and}$$

$$\boldsymbol{D}^*=(\boldsymbol{A}^*-\boldsymbol{I})\boldsymbol{A}^{-1}\boldsymbol{D}$$

3. OPTIMAL CONTROL

Using the control force $\boldsymbol{U}$ and the state variable $\boldsymbol{Q}^*$ at each time step i, the objective function J is specified as below

$$J(\boldsymbol{Q}^*,\boldsymbol{U})=\frac{1}{2}\sum_{i=0}^{\infty}(\boldsymbol{Q}_i^{*T}\widehat{\boldsymbol{R}}_Q\boldsymbol{Q}_i^*+\boldsymbol{U}_i^T\widehat{\boldsymbol{R}}_U\boldsymbol{U}_i)\quad\cdots\cdots(13)$$

The diagonal matrices $\widehat{\boldsymbol{R}}_Q$ and $\widehat{\boldsymbol{R}}_U$ are positive weight functions and represented by

$$\widehat{\boldsymbol{R}}_Q=r_Q\boldsymbol{I}\qquad\widehat{\boldsymbol{R}}_U=r_U\boldsymbol{I}\quad\cdots\cdots(14)$$

Following the assumption[2] that the ratio of the aerodynamic forces to the inertial and spring forces is small, we neglect the aerodynamic force term $\boldsymbol{F}_{e,i-1}$ in minimization, moreover as these terms are the function of structural velocity, they will be minimized with the minimization of state vector $\boldsymbol{Q}^*$. Hence in accordance with the optimal control law, $J(\boldsymbol{Q}^*,\boldsymbol{U})$ has its minimum value when the matrix $\boldsymbol{P}$ satisfies the stationary Riccati equation[16]

$$\boldsymbol{P}=\widehat{\boldsymbol{R}}_Q+\boldsymbol{A}^{*T}\boldsymbol{P}\boldsymbol{A}^*-\boldsymbol{A}^{*T}\boldsymbol{P}\boldsymbol{C}^*(\widehat{\boldsymbol{R}}_U+\boldsymbol{C}^{*T}\boldsymbol{P}\boldsymbol{C}^*)^{-1}\boldsymbol{C}^{*T}\boldsymbol{P}\boldsymbol{A}^*\quad\cdots\cdots(15)$$

The magnitude of optimal control force $\boldsymbol{U}_i$ at each time step i is given by[16]

$$\boldsymbol{U}_i=-\boldsymbol{E}_A\boldsymbol{Q}_i^*-\boldsymbol{E}_D\boldsymbol{F}_{e,i-1}\quad\cdots\cdots(16)$$

As the buffeting force can not be predicted before hand, it is not included in the control force equation (16), while the coefficient matrices $\boldsymbol{E}_A$ and $\boldsymbol{E}_D$ are given by

$$\boldsymbol{E}_A=(\widehat{\boldsymbol{R}}_U+\boldsymbol{C}^{*T}\boldsymbol{P}\boldsymbol{C}^*)^{-1}\boldsymbol{C}^{*T}\boldsymbol{P}\boldsymbol{A}^*\quad\cdots\cdots(17a)$$

$$\boldsymbol{E}_D=(\widehat{\boldsymbol{R}}_U+\boldsymbol{C}^{*T}\boldsymbol{P}\boldsymbol{C}^*)^{-1}\boldsymbol{C}^{*T}\boldsymbol{P}\boldsymbol{D}^*\quad\cdots\cdots(17b)$$

4. OBSERVER EQUATION

The state Eq. (12) can predict the actual value of state vector $\boldsymbol{Q}_{i+1}^*$, only when the gust force is known. In actual practice the gust force cannot be predicted and hence neglecting the gust force will give a different value of state vector $\bar{\boldsymbol{Q}}_{i+1}^*$. When this simulated value of state vector along with the self-exciting aerodynamic force is used for the calculation of control force, the controller may not be able to control the structure effectively. This problem can be circumvented by the introduction of an observer[17].

Let us consider that κ sensors are attached for measuring the actual response $\boldsymbol{Y}_i$, then the observer equation is given as

$$\boldsymbol{Y}_i=\boldsymbol{G}\boldsymbol{Q}_i^*\quad\cdots\cdots(18)$$

where $\boldsymbol{G}$ is a $\kappa\times 4$ matrix used for connecting the measured value of displacement vector to the state vector. The state equation and the control force equation without the observer are given as

$$\bar{\boldsymbol{Q}}_{i+1}^*=\boldsymbol{A}^*\bar{\boldsymbol{Q}}_i^*+\boldsymbol{C}^*\boldsymbol{U}_i+\boldsymbol{D}^*\bar{\boldsymbol{F}}_{e,i-1}\quad\cdots\cdots(19a)$$

$$\boldsymbol{U}_i=-\boldsymbol{E}_A\bar{\boldsymbol{Q}}_i^*-\boldsymbol{E}_D\bar{\boldsymbol{F}}_{e,i-1}\quad\cdots\cdots(19b)$$

The difference between the $\boldsymbol{Q}_i^*$ and $\bar{\boldsymbol{Q}}_i^*$ is adjusted by minimizing the difference between the real displacement $\boldsymbol{Y}_i$ and the simulated displacement $\bar{\boldsymbol{Y}}_i$. This minimization is achieved by introducing an adjustment matrix $\boldsymbol{L}$ in the state Eq. (19a) as follows

$$\bar{Q}_{i+1}^{*}=A^{*}\bar{Q}_{i}^{*}+C^{*}U_{i}+D^{*}\bar{F}_{e,i-1}+LG(Q_{i}^{*}-\bar{Q}_{i}^{*}) \quad \cdots\cdots(20)$$

Substituting Eq. (19b) in Eq. (13), the objective function J is modified as follows

$$J=\frac{1}{2}\sum_{i=0}^{\infty}[\,Q_{i}^{*T}\hat{R}_{Q}Q_{i}^{*}+(-E_{A}\bar{Q}_{i}^{*})^{T}\hat{R}_{U}(-E_{A}\bar{Q}_{i}^{*}) \quad \cdots\cdots(21)$$

In Eq. (21) the aerodynamic force $\bar{F}_{e,i-1}$ has been neglected as it is very small compared to the inertial and elastic forces. Again, since the effect of buffeting force can be taken into account through observer, it is also neglected. With this consideration, Eq. (21) can be written as[16]

$$J=\frac{1}{2}[\,Q_{0}^{*T}PQ_{0}^{*}+(Q_{0}^{*}-\bar{Q}_{0}^{*})^{T}\Pi(Q_{0}^{*}-\bar{Q}_{0}^{*})]$$

$$=J_{\min}+\Delta J \quad \cdots\cdots(22)$$

where

$$J_{\min}=\frac{1}{2}Q_{0}^{*T}PQ_{0}^{*} \quad \cdots\cdots(23a)$$

$$\Delta J=\frac{1}{2}(Q_{0}^{*}-\bar{Q}_{0}^{*})^{T}\Pi(Q_{0}^{*}-\bar{Q}_{0}^{*}) \quad \cdots\cdots(23b)$$

where subscript 0 is the initial value at time step $i=0$. Matrix P is a solution of the stationary Riccati Eq. (15), and parameter Π satisfies the equation

$$\Pi=\Pi_{0}+(A^{*}-LG)^{T}\Pi(A^{*}-LG) \quad \cdots\cdots(24)$$

where

$$\Pi_{0}=E_{A}^{T}(\hat{R}_{U}+C^{*T}PC^{*})E_{A}$$

5. OPTIMAL OBSERVER THAT MINIMIZES ΔJ

We will now introduce an observer which minimizes the increase ΔJ in Eq. (22). Let Q_{0}^{*} be a hypothetical vector with zero mean and unit variance as

$$E[\,Q_{0}^{*}]=0, \qquad E[\,Q_{0}^{*}\cdot Q_{0}^{*T}]=I_{4} \quad \cdots\cdots(25)$$

Let $\bar{Q}_{0}^{*}=0$, then the expected value of ΔJ is given as follows,

$$E[\,\Delta J]=E[\,Q_{0}^{*T}\Pi Q_{0}^{*}]=trace\Pi \quad \cdots\cdots(26)$$

For the minimization, we add the constraint Eq. (24), by introducing Lagrange multipliers Λ in Eq. (26).

$$\bar{J}=E[\,\Delta J]+trace[\,\Lambda^{T}\{-\Pi+\Pi_{0}+(A^{*}-LG)^{T}\Pi(A^{*}-LG)\}] \quad \cdots\cdots(27)$$

Minimizing $\bar{J}$ with L and Π[18] we get,

$$\frac{\partial\bar{J}}{\partial L}=-\Pi^{T}A^{*}\Lambda G^{T}-\Pi A^{*}\Lambda^{T}G^{T}+\Pi^{T}LG\Lambda G^{T}+\Pi LG\Lambda^{T}G^{T}=0$$

$$L=A^{*}\Lambda G(G\Lambda G^{T})^{-1} \quad \cdots\cdots(28)$$

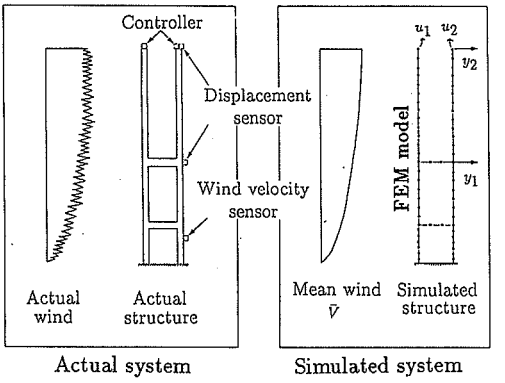

Fig.1 Control system layout with observer

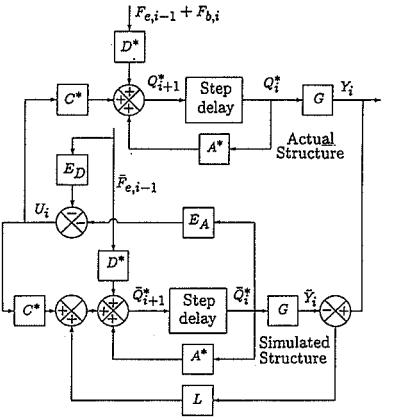

Fig.2 Block diagram for control system with observer

$$\frac{\partial\bar{J}}{\partial\Pi}=I-A^{T}+(A^{*}-LG)\Lambda(A^{*}-LG)^{T}=0$$

$$\Lambda=I+A^{*}\Lambda A^{*T}-A^{*}\Lambda G^{T}(G\Lambda G^{T})^{-1}G\Lambda A^{*T} \quad \cdots\cdots(29)$$

6. CONTROL SYSTEM LAYOUT WITH OBSERVER

Two systems are shown in **Fig.1**. The actual system and the computer simulated system. The actual system is subjected to a natural wind force. In this study, the natural wind force is assumed to consist of two components. The self-excited force which corresponds to the mean velocity $V(z)$ of the wind and the gust load which is due to the fluctuating wind velocity components ($v_{b}(z,t)$ and $w_{b}(z,t)$). This model of the natural wind force will be referred as the actual wind force hereafter. The simulated system represents a prototype of the actual structure. This system is subjected to a self-excited force due to the mean velocity $\bar{V}(z)$. The difference in the mean velocities of the two systems has been assumed to take into account the measurement error of the mean velocity and also

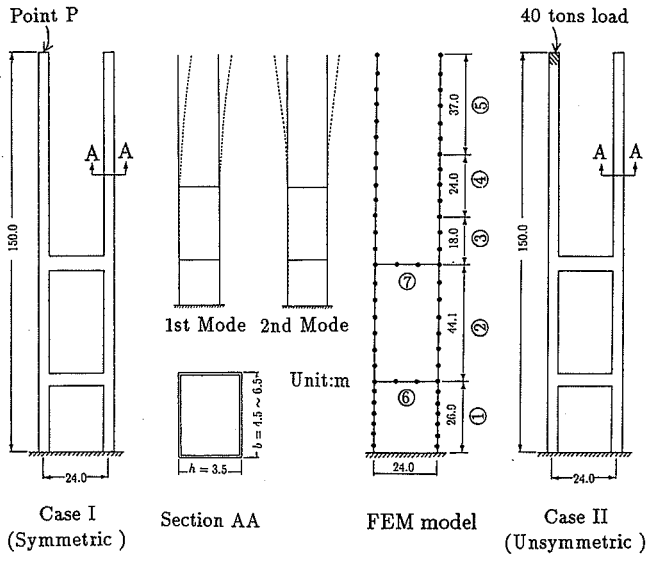

Fig.3 Dimensions, FEM mesh and mode shapes of the simulated structure

Table 1 Structural Properties of Tower

Segment Number	Mass per unit Length t/m	Moment of Inertia m^4
①	16.273	2.45
②	10.921	2.35
③	16.840	2.50
④	13.706	1.808
⑤	13.353	0.957
⑥	7.696	4.435
⑦	9.812	6.966

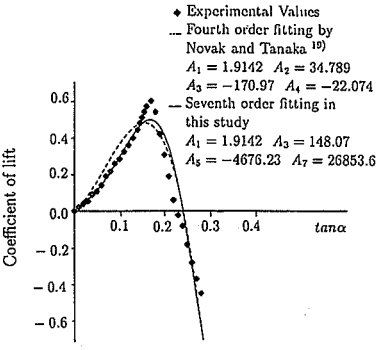

Fig.4 Coefficient of lift of a 2:3 rectangular section in a smooth flow

Table 2 Vibration Properties of the Two Cases

Vibration Properties	Case I		Case II	
	Mode-1	Mode-2	Mode-1	Mode-2
Circular frequency (rad/s)	2.79	2.99	2.66	2.92
Damping ratio	0.0016	0.0014	0.0016	0.0014
Mass ratio	0.000163	0.000167	0.000146	0.000164
Galloping onset velocity (m/s)	16.3	14.8	17.3	14.8

the uncertainty in the prediction of self-induced force. **Fig.2** shows the block diagram of the control algorithm with an observer corresponding to Eqs. (12), (19b) and (20).

7. NUMERICAL RESULTS AND COMPARISONS

Description of structure :

Pheinsusom and Fujino[3], while describing the multimode galloping behavior in structures having closely-spaced natural frequencies, showed that if the structural properties are symmetric, galloping is always a single mode phenomenon. On the other hand, if the structural properties are unsymmetric, such as unsymmetrically distributed mass or non-uniform cross section, galloping is a multimode phenomenon. With this consideration, we adopted similar structures to that used in reference[3] for our study. Here we denoted the structure with symmetric properties as Case I and that with unsymmetric properties as Case II and described below.

Case I (Structure with symmetric properties) :

We have considered a tower similar to the Higashi Kobe bridge tower. The dimensions and the FEM model of the simulated tower is shown in **Fig.3** and its corresponding structural properties are given in **Table 1**. For simplicity, the structural properties, as shown in **Table 1**, are modified as the piecewise average values to the actual values of the tower. Also in this study, only the in-plane vibration of the tower is considered. As the in-plane motion of the tower is not much affected by the presence of cables, and also as the effect of vertical in-plane motion is very little on the lateral motion and rotation, their effects are neglected. Hence each element is modeled with a beam element having two degrees of freedom namely an in-plane horizontal displacement and a rotation. The first two natural frequencies of this simulated tower are found to be 2.79 rad/s and 2.99 rad/s respectively. As these frequencies are considerably close to each other, they are selected to observe the multimode galloping behavior of the bridge tower. The corresponding mode shapes are also shown in **Fig.3**. The eigen modes are normalized by the eigen mode component at the top of the tower at point P. The modal damping ratios for the two modes are assumed to be 0.0016 and 0.0014[3] respectively. The mass ratio for the two modes are found to be 1.63×10^{-4} and 1.67×10^{-4} . The vibration properties of the tower are shown in

Table 3 Aerodynamic Co-efficient for the Two cases

Aerodynamic Coefficients	Case I		Case II	
	Mode-1	Mode-2	Mode-1	Mode-2
$C_{A,*1}$	3.08×10^{0}	3.09×10^{0}	3.08×10^{0}	3.09×10^{0}
$C_{A,*2}$	8.06×10^{-1}	-1.00×10^{-10}	4.77×10^{0}	-4.15×10^{0}
$C_{A,*3}$	-8.80×10^{-11}	8.73×10^{-1}	-5.82×10^{-1}	1.51×10^{0}
$C_{A,*4}$	7.68×10^{-1}	4.58×10^{-11}	2.12×10^{-1}	6.37×10^{-1}
$C_{A,*5}$	4.03×10^{-11}	8.37×10^{-1}	8.93×10^{-2}	7.43×10^{-1}
$C_{A,*6}$	2.58×10^{-1}	-6.19×10^{-11}	1.00×10^{1}	-1.05×10^{1}
$C_{A,*7}$	-5.45×10^{-11}	2.85×10^{-1}	-1.48×10^{0}	1.89×10^{0}
$C_{A,*8}$	2.51×10^{-1}	-1.44×10^{-11}	2.65×10^{-1}	-1.77×10^{-3}
$C_{A,*9}$	-1.27×10^{-11}	2.77×10^{-1}	-2.48×10^{-4}	2.80×10^{-1}
$C_{A,*10}$	2.44×10^{-1}	3.06×10^{-11}	3.93×10^{-2}	2.33×10^{-1}
$C_{A,*11}$	2.69×10^{-11}	2.71×10^{-1}	3.26×10^{-2}	2.35×10^{-1}
$C_{A,*12}$	8.96×10^{-2}	-3.19×10^{-11}	2.34×10^{1}	2.54×10^{1}
$C_{A,*13}$	-2.81×10^{-11}	1.00×10^{-1}	-3.56×10^{0}	3.97×10^{0}
$C_{A,*14}$	8.80×10^{-2}	-1.53×10^{-11}	5.57×10^{-1}	-5.06×10^{-1}
$C_{A,*15}$	-1.35×10^{-11}	9.83×10^{-2}	-7.10×10^{-2}	1.77×10^{-1}
$C_{A,*16}$	8.65×10^{-2}	7.40×10^{-13}	2.47×10^{-2}	7.11×10^{-2}
$C_{A,*17}$	6.51×10^{-13}	9.68×10^{-2}	9.97×10^{-3}	8.60×10^{-2}
$C_{A,*18}$	8.51×10^{-2}	1.62×10^{-11}	1.21×10^{-2}	8.27×10^{-2}
$C_{A,*19}$	1.43×10^{-11}	9.53×10^{-2}	1.16×10^{-2}	8.21×10^{-2}
$C_{U,*1}$	4.00×10^{-2}	-4.54×10^{-2}	2.78×10^{-2}	-3.07×10^{-2}
$C_{U,*2}$	4.00×10^{-2}	4.54×10^{-2}	1.08×10^{-2}	7.66×10^{-2}

* indicates the mode number

Table 2.

Because of the unavailability of the aerodynamic coefficients A_1, A_3, A_5 and A_7 of this cross section of tower in the literature, and since the tower legs are similar to the 2:3 rectangular section, the aerodynamic coefficients are assumed to be that of a 2:3 rectangular section. These coefficients are obtained by the curve fitting of the coefficient of lifts for a 2:3 rectangular section[19] and are shown in **Fig.4**. Although the coefficient of lift in a gusty wind is different than smooth wind[19], in this study, for expediency, we have used the same coefficients for both smooth and gusty wind. The coefficients $C_{A,nk}$ and $C_{U,nj}$ (two controllers on the top of each leg of the tower) are shown in **Table 3**. The critical wind velocities ($V_{crn}=\beta_n\omega_n h/\mu_n C_{A,n1}A_1$) for the onset of galloping of two modes are calculated to be 16.3 m/s and 14.8 m/s respectively (at the tower top 25.5 m/s and 23.3 m/s respectively, with $p=1/6$).

Case II (Structure with unsymmetric properties) :

To observe the multimodal galloping behavior, we added an additional 40 ton load to one of the legs of the actual tower to make its mass distribution unsymmetric as shown in **Fig.3**. The additional load may be considered as a crane mounted on one of the legs of the tower during its construction[3]. The first two in-plane natural frequencies of this modified tower have been changed to 2.66 rad/s and 2.92 rad/s, respectively. The mass ratio for the two modes are found to be 1.46×10^{-4} and 1.64×10^{-4} respectively. The coefficients $C_{A,nk}$ and $C_{U,nj}$ for this tower are shown in **Table 3**.

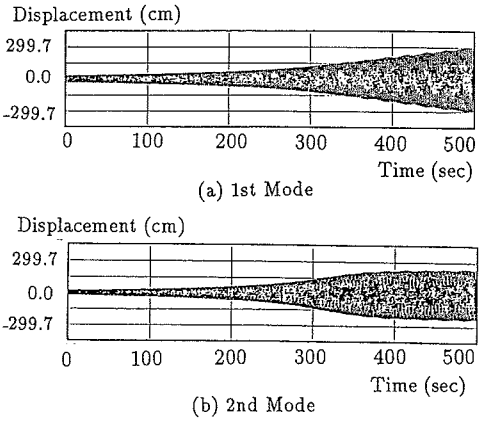

Fig.5 Time history response of Case II in smooth flow

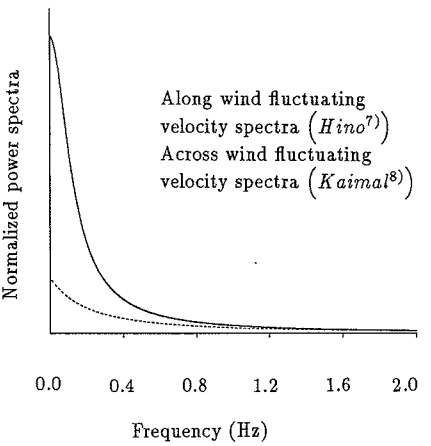

Fig.6 Along and across wind fluctuating velocities power spectra ($z=10$ m)

(1) Galloping Phenomenon

CaseI : The simulated tower with symmetric structure and mass distribution is examined for galloping behavior under smooth flow with a mean velocity at reference height as $V_0=35$ m/s (tower top velocity=55 m/s). For the various combination of initial excitations it is found that the galloping is always a single mode phenomenon. The steady-state value depends on the initial mode of excitation.

Case II : The modified tower is also checked for the galloping behavior at the same wind velocity *i.e.* $V_0=35$ m/s under smooth flow. We checked several cases and found that galloping is always a multimode phenomenon irrespective of the initial disturbance which is in accordance with reference[3]. However, because of lack of space we have not reported all the cases and only a typical example is shown in **Fig.5**, where the tower is excited in the

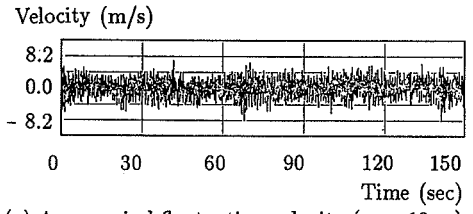

(a) Across wind fluctuating velocity ($z = 10\ m$)

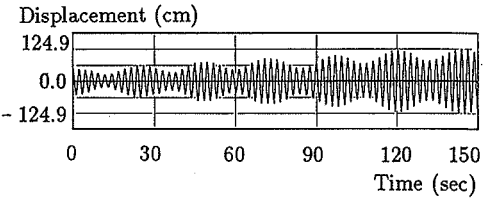

(b) Vibration without control

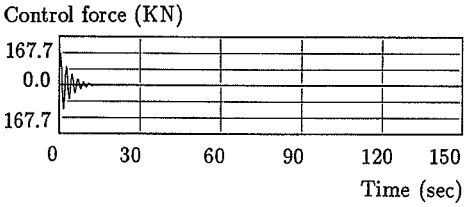

(c) Control force without observer

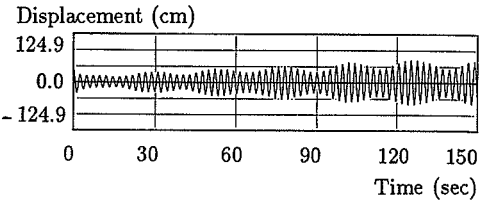

(d) Controlled vibration without observer

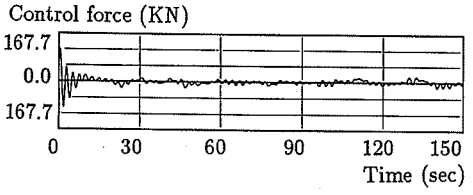

(e) Control force with observer

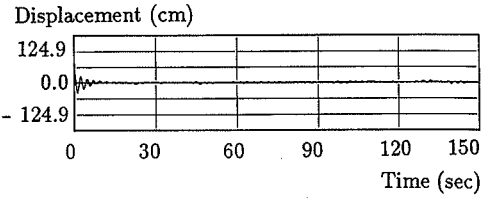

(f) Controlled vibration with observer

Fig.7 Time history of across wind fluctuating velocity, uncontrolled and controlled displacement responses and control forces at the top of tower$\left(\frac{\hat{R}_Q}{\hat{R}_U}=3.0\times10^{10}\right)$

mixed mode and the simultaneous galloping of two modes leads to a multimodal galloping.

(2) Galloping Control

For the galloping control, we considered several examples of Case Ⅰ and Case Ⅱ, and in all cases we obtained a reasonably good performance of the proposed control scheme with an observer. Again lack of space restricted us to include all the cases and only the galloping control of the modified tower (Case Ⅱ) is included in the illustrative example. However, in the parametric study, the results of both cases have been included.

In the illustrative example, we assumed that the control system is not fed with the information about the mass change. Hence our simulated structure corresponds to Case Ⅰ and the actual structure corresponds to Case Ⅱ. To show the uncertainty in the mean velocity measurement and the aerodynamic force prediction, it is supposed that the controller assumes a mean velocity of 25 m/s instead of 35 m/s. This introduces a discrepancy between the measured and the actual values of the mean velocity. There are two displacement sensors, one at the top and the other at nearly mid height of the tower as shown in **Fig.1** and two controllers are placed on the top of each leg of the tower also shown in **Fig.1**.

For the gust load, the surface drag coefficient is assumed to be $K=0.003$[12]. The power spectral densities of the fluctuating winds, at the reference height $z=10$ m are shown in **Fig.6**. Again because of the unavailability of actual C_L and C_L' for this section of tower in the literature, we have conservatively assumed C_L' as the slope of steepest part of **Fig.4** . Which is approximately 8.0 and C_L $=0.4$ ($C_L'=4.22$ and $C_L'=0.27$ for bridge deck[11]).

The tower is excited in the mixed mode and the time history of across wind fluctuating velocity, responses and the control forces are shown in **Fig.7**. **Fig.7**(a) shows the across wind fluctuating velocity at the reference height $z_0=10$ m. Similarly **Figs.7**(b), 7(f) and 7(d) show the uncontrolled and controlled vibration at the top of tower at point P with and without observer respectively. It can be seen from **Fig.7** (d), that in the absence of an observer, the control scheme is not very effective, this is because of the reason that the controller is unable to predict the actual response of the

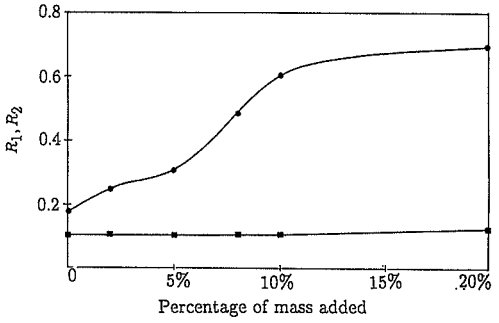

(a) Effect of mass variation on control scheme (Case I)

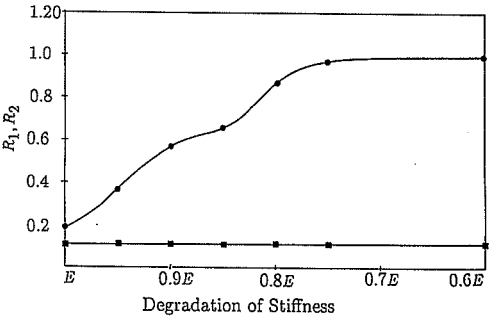

(b) Effect of stiffness degradation on control scheme (Case I)

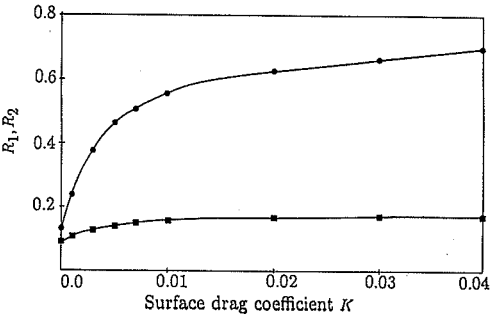

(c) Effect of gust intensity on control scheme (Case II)

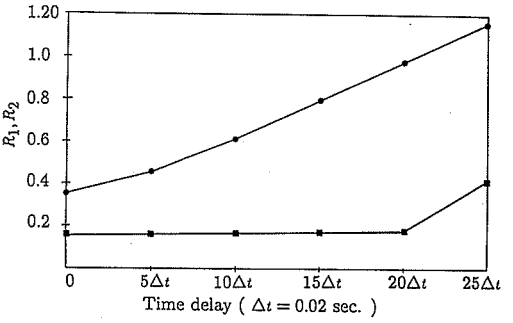

(d) Effect of time delay on control scheme (Case II)

$$*R_1 = \frac{\text{rms value of controlled vibration without observer after 150 sec.}}{\text{rms value of uncontrolled vibration after 150 sec.}}$$

$$*R_2 = \frac{\text{rms value of controlled vibration with observer after 150 sec.}}{\text{rms value of uncontrolled vibration after 150 sec.}}$$

Fig.9 Effect of the observer on the system mass and stiffness changes, gust intensity and the time delay

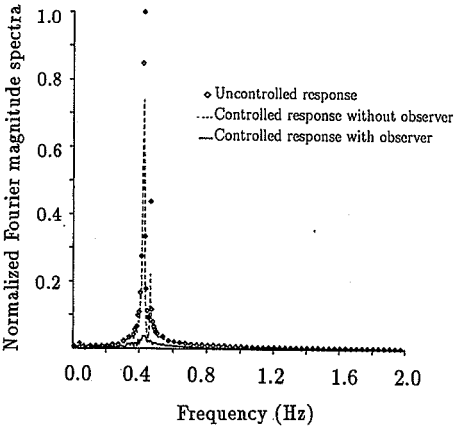

Fig.8 Fourier magnitude spectra of uncontrolled and controlled displacements with and without observer after 150 sec.

structure and the control force (controller location at point P) approaches to zero as shown in **Fig.7**(c). Whereas in the presence of an observer, the controller can predict the actual response more correctly and hence can accurately calculate the control force as shown in **Fig.7**(e). The corresponding power spectra is shown in **Fig.8**. The geometrical figure, the firm line and the dotted line show the power spectra of uncontrolled, controlled vibrations with and without an observer respectively. The peaks at 0.42 Hz and 0.46 Hz are due to the first and the second natural modes of vibration.

(3) Parametric Study

A parametric study is also carried out to see the effect of an observer at different turbulence intensities and the change in system parameters such as stiffness and mass matrices. The time delay effect on the performance of control scheme is also investigated. Following are the results of this parametric study

1. **Figs.9**(a) and **9**(b) show the effect of change

in system mass and stiffness respectively on the controlled response with and without an observer. For the system with mass change, we assumed the symmetric structure (Case Ⅰ) as the simulated structure and the actual structure is simulated by adding a percentage of each nodal mass to the corresponding mass. Results are plotted between R_1, R_2 and percentage mass change as shown in **Fig.9**(a). Where R_1 is the ratio of the *rms* value of the controlled vibration without an observer to that of the *rms* value of uncontrolled vibration. Similarly R_2 is the ratio of the *rms* value of controlled vibration with an observer to that of the *rms* value of uncontrolled vibration. All *rms* values corresponds to 150 sec. measurement. It can be seen that the performance of the controller scheme without an observer deteriorates continuously, whereas, there is a very little change in the performance of controlled vibration with an observer. Similarly, in case of system stiffness change, we simulated the actual structure having certain degradation in the modulus of elasticity E. The results are shown in **Fig.9**(b) in terms of R_1, R_2 and the degradation of stiffness (E). The inspection of **Fig.9** (b) reveals the same trend as that of **Fig.9** (a).

2. **Fig.9**(c) shows the effect of an observer at different turbulence intensities. For this purpose, we considered the modified tower (Case Ⅱ). To observe the effect of turbulence intensity more effectively, we assumed that the controller is maintaining the full knowledge of the change in the system mass matrix. In other words, our simulated structure is also the modified tower (Case Ⅱ). The intensity of turbulence is characterized by the surface drag coefficient K. Again the results are plotted between R_1, R_2 and K values, where R_1 and R_2 have the same meaning as defined earlier. It can be seen from **Fig.9**(c) that with the increase in turbulence intensity the increase in R_2 value is very small, whereas the increase in R_1 value is appreciably large.

3. **Fig.9**(d) shows the effect of time delay on the controlled response with and without an observer. For this study, both simulated and actual structures correspond to Case Ⅱ. From **Fig.9**(d), It can be seen that the performance of the controller scheme without observer deteriorates continuously, whereas in the scheme with an observer, the change is almost negligible until a time lag of 20 Δt (Δt=0.02 sec.). However, when the time delay reaches a value of 25 Δt, a deterioration in performance takes place. It can be noted that at 25 Δt, the time lag is 0.50 sec., which is nearly equal to one-fourth value of the time periods of first and second modes which are 0.59 sec. and 0.54 sec. respectively. Thus, when the time lag reaches one-fourth value of any of the controlled modes, the proposed system performance deteriorates. The time delay problem in higher modes consideration, where the time periods of the modes are smaller, can be avoided by considering a smaller sampling time Δt.

8. CONCLUSIONS

An active optimal control algorithm with an optimal observer is presented for the control of a bridge tower subjected to galloping in a gusty wind. The following conclusions are drawn

1. The proposed control scheme with an observer is found to be effective for both the single and multimode galloping control problem. The scheme is found to be robust against the uncertainty due to the prediction in the aerodynamic forces and the gust forces.

2. The proposition is efficient to account for the inherent effect of aging of the structure, which leads to a spontaneous variation in the system parameters, such as change in mass or stiffness matrix. Moreover, it is found to be equally efficient against the effect of occasional unsymmetric mass distribution. The presence of an observer also makes the control scheme robust against time delay. However, a large time delay resuls in the deterioration of scheme, which can be compensated by taking a smaller sampling period.

ACKNOWLEDGMENT

The writers wish to express their special gratitude to Prof. M. Suzuki and Mr. D. Baldelli of Nagoya University (Aeronautical Dept.) for their invaluable advice and contributing suggestions. Mr. A. Usman and Mr. K. Yabunaka are acknowledged for their assistance in the preparation of the manuscript.

Appendix 1. Analysis of Buffeting Force

From Eq. (5) the mean square value of buffeting force for n th mode is given as[13)~15)]

$$\overline{F_{bn}^2(t)}=\frac{1}{m_n^2 D_n^2}\int_0^l\int_0^l \overline{F_b(z,t)F_b(z',t)} \cdot \Psi_n(z)\Psi_n(z')dzdz' \quad \cdots\cdots\cdots (A.1)$$

where bar denotes the time averages. $\overline{F_b(z,t)F_b(z',t)}$ represents the covariance of the buffeting force at points z and z'. Substituting Eqs. (3) and (4b) in Eq. (A.1) and neglecting the cross terms due to along and across wind fluctuating velocities[13)], we get

$$\overline{F_{bn}^2(t)}=\frac{1}{m_n^2 D_n^2}\int_0^l\int_0^l\left(\frac{1}{2}\rho h V_0\right)^2 v(z)v(z')$$

$$\cdot[(2C_L)^2\overline{v_b(z,t)v_b(z',t)}+(C_L')^2 \overline{w_b(z,t)w_b(z',t)}]\cdot\Psi_n(z)\Psi_n(z')dzdz' \quad \cdots\cdots (A.2)$$

But

$$\overline{v_b(z,t)v_b(z',t)}=2\int_0^\infty S_{vv}(\omega)\sqrt{COH}\,d\omega$$

$$\overline{v_b(z,t)v_b(z',t)}=2\int_0^\infty S_{vv}(\omega)\cdot\exp\left(-k_1\frac{\omega}{2\pi V_0}\Delta z\right)d\omega \quad \cdots\cdots (A.3)$$

Similarly

$$\overline{w_b(z,t)w_b(z',t)}=2\int_0^\infty S_{ww}(\omega)\cdot\exp\left(-k_1\frac{\omega}{2\pi V_0}\Delta z\right)d\omega \quad \cdots\cdots (A.4)$$

where COH is defined as the coherence function and k_1 is the decay factor. Δz is the separation of points z and z'. Substituting Eqs. (A.3) and (A.4) in Eq. (A.2), we get

$$\overline{F_{bn}^2(t)}=\left(\frac{2\mu_n}{h}\frac{1}{D_n}\right)^2\int_0^l\int_0^l v(z)v(z')\Psi_n(z)\Psi_n(z')\cdot\left[(2V_0C_L)^2 2\int_0^\infty S_{vv}(\omega)\cdot\exp\left(-k_1\frac{\omega}{2\pi V_0}\Delta z\right)d\omega+(V_0C_L')^2 2\cdot\int_0^\infty S_{ww}(\omega)\exp\left(-k_1\frac{\omega}{2\pi V_0}\Delta z\right)d\omega\right] dzdz' \quad \cdots\cdots (A.5)$$

Eq. (A.5) can be simplified as

$$\overline{F_{bn}^2(t)}=\left(\frac{2\mu_n}{h}\right)^2\left\{(2V_0C_L)^2 2\int_0^\infty S_{vv}(\omega)\cdot|J_n(\omega)|^2d\omega+(V_0C_L')^2 2\int_0^\infty S_{ww}(\omega)\cdot|J_n(\omega)|^2d\omega\right\} \quad \cdots\cdots (A.6)$$

where

$$|J_n(\omega)|^2=\frac{1}{D_n^2}\int_0^l\int_0^l v(z)v(z')\Psi_n(z)\Psi_n(z')\cdot\exp\left(-k_1\frac{\omega}{2\pi V_0}\Delta z\right)dzdz' \quad \cdots\cdots (A.7)$$

Introducing aerodynamic admittances $\gamma_1(\omega)$ and $\gamma_2(\omega)$[12),13)] in Eq. (A.6), we get

$$\overline{F_{bn}^2(t)}=\left(\frac{2\mu_n}{h}\right)^2\left\{(2V_0C_L)^2 2\int_0^\infty S_{vv}(\omega)|\gamma_1(\omega)|^2\cdot|J_n(\omega)|^2d\omega+(V_0C_L')^2 2\int_0^\infty S_{ww}(\omega)\cdot|\gamma_2(\omega)|^2|J_n(\omega)|^2d\omega\right\} \quad \cdots\cdots (A.8)$$

where $\gamma_1(\omega)$ and $\gamma_2(\omega)$ are given as

$$|\gamma_1(\omega)|^2=|\gamma_2(\omega)|^2=\frac{2[\bar\lambda b-1+\exp(-\bar\lambda b)]}{(\bar\lambda b)^2} \quad \cdots\cdots (A.9)$$

where $\bar\lambda=-k_1\omega/2\pi V_0$ and b is the dimension of the tower along the wind direction as shown in **Fig.3**. Eq. (A.8) in time domain can be simulated as

$$F_{bn}(t)=\frac{2\mu_n}{h}f_{bn}(t) \quad \cdots\cdots (A.10)$$

where

$$f_{bn}(t)=2V_0C_L\left\{\sqrt{2}\sum_{j=1}^N[S_{vv}(\omega_j)|\gamma_1(\omega_j)|^2\cdot|J_n(\omega_j)|^2\Delta\omega]^{\frac{1}{2}}\cos(\omega_jt+\phi_j)\right\}+V_0C_L'\cdot\left[\sqrt{2}\sum_{j=1}^N[S_{ww}(\omega)|\gamma_2(\omega_j)|^2\cdot|J_n(\omega_j)|^2\Delta\omega]^{\frac{1}{2}}\cos(\omega_jt+\varphi_j)\right] \quad \cdots\cdots (A.11)$$

REFERENCES

1) Fujino, Y., Warnitchai, P. and Ito, M. : Suppression of Galloping of Bridge Tower Using Tuned Mass Damper, Journal of the Faculty of Engineering, the University of Tokyo (B), Vol.38, No.2, pp.49~73, 1985.
2) Blevins, R.D. and Iwan, W.D. : The Galloping Response of a Two Degree of Freedom System, Journal of Applied Mechanics, Transaction of ASME, pp.1113~1118, 1974.
3) Pheinsusom, P. and Fujino, Y. : Galloping of Structure with Two Closely-Spaced Natural Frequencies, Proc. of JSCE, No.392/I-9, pp.215~225, 1988.
4) Pheinsusom, P. and Fujino, Y. : Effect of Turbulence on the Modal Interaction in Galloping of Structure with Two Closely-Spaced Natural Frequencies (Technical Note), Proc. of JSCE, No.398/I-10, pp.193~196, 1988.
5) Balas, M. J. : Direct Velocity Feedback Control of Large Space Structures (Engineering Notes) J. Guidance and Control, Vol.2, No.3, pp.252~253, 1979.
6) Tsuchiya, K., Kashiwaze, T. and Manabe, S. : Position Control of a Flexible Satellite, Journal of the Society of Instrument and Control Engineers, Vol.24, No.5, pp.410~416 (in Japanese), 1985.
7) Hino, M. : Spectrum of Gusty Wind, Papers 1-7-2, Proceedings, Third International Conference on Buildings and Structures, Tokyo, Japan, 1971.
8) Kaimal, J. C., Wyngaard, J. C., Izumi, Y., and Cote, O. R. : Spectral Characteristics of Surface-Layer Turbulence, Quarterly Journal of Meteorological Society 98, pp.563~589, 1972.
9) Parkinson, G.V. and Smith, J.D. : The Square Prism as an Aeroelastic Non-Linear Oscillator, Quarterly Journal of Mechanics and Applied Mathematics 17, pp.225~239, 1964.

10) Otsuki, Y., Washizu, K., Tomizawa, H. and Ohya, A. : A Note on the Aeroelastic Instability of a Prismatic Bar with Square Section, Journal of Sound and Vibration, Vol.34, No.2, pp.233～248, 1974.
11) Scanlan, R. H. and Nicholas, P. J. : Aeroelastic Analysis of Cable-Stayed Bridges. Journal of Structural Engineering, ASCE , Vol.116, No.2, pp.279～297, 1990.
12) Beliveau, J. G., Vaicaitis, R. and Shinozuka, M. : Motion of Suspension Bridge Subject to Wind Loads, Journal of Structural Engineering, ASCE, ST6, pp.1189～1205, 1977.
13) Davenport, A. G. : The Response of Slender, Line-Like Structures to a Gusty Wind. Proceedings, Institution of Civil Engineers, London, England, Vol.23, pp.389～408, 1962.
14) Masao, S. : Characteristic of Strong Wind, Tokyo, Japan (in Japanese), 1981.
15) Ishizaki, H. : Wind Engineering, Tokyo, Japan (in Japanese), 1977.
16) Ogata, K. : Discrete-Time Control Systems. Englewood Cliffs, NJ, Prentice-Hall,Inc., pp.625～881, 1987.
17) Baba, S., Ninomiya, K. and Hayashi Y. : Active Optimal Control of Structure Using Optimal Observer. Journal of Engineering Mechanics, ASCE, Vol.115, No.11, pp.2564-2581, 1989.
18) Mita, T. and Mukaida, M. : Parallel Computation in Digital Feedback Control System. Trans. of the Soc. of Instrument and Control Engineering, Vol.18, N0.6, pp.556～563 (in Japanese), 1982.
19) Novak, M. and Tanaka, H. : Effect of Turbulence on Galloping Instability, Journal of Engineering Mechanics, ASCE, Vol.100, No.1, pp.27～47, 1974.

(Received March 31, 1992)

最適オブザーバを用いた橋塔のギャロッピングに対する最適制御

S. M. Shahid ALAM・馬場俊介・松本　勝

長大橋の主塔に発生するギャロッピングのような，自励振動を抑制する動的最適制御法について示している．空気力をモデル化するために，準定常理論を用い，モード間の連成を観察するためにマルチモード応答を考慮している．ガスト荷重をランダム現象と考え，風の方向および直角の風速変動のパワースペクトルでモデル化する．準定常理論の不確定性とランダムガスト現象に起因する応答予測の誤差は，オブザーバーの導入により修正する．目的関数の増加を最小にするために最適オブザーバーを用いる．システムパラメーターとガスト強度の変化に対するオブザーバーの効果，およびコントローラーの時間遅れの制御におよぼす効果についても調べる．